

### 6.9.4.3. Destruction energy of RL(T)

The destruction of RL(T) has the following specific features:

- The destruction energy of RL(T) is larger than the destruction energy of RL(R)
- The CL space exhibits asymmetric behaviour: the destruction energy of +RL(T) is the larger than the destruction energy of -RL(T) (as was discussed in §6.9.4.2).

The antipressure balance between both types of RL(R) is valid for the volume ratio, established during the phase of the crystalization. The process of twisting (volume shrinking), however, disturbs this ratio. This is evident from Fig. 6.9 and Eq. (6.8). Then the antipressure for the both types of RL(T) appears different.

The twisting causes shrinking of the small radius of FOHS, but the relative change is small. It is given by  $k_S$  coefficient, determined by the ratio of muon to pion Newtonian masses. If assuming, that the twisting of the internal pion is quite small, the factor  $k_S$  should be approximately valid, when used for RL(T) of the electron (positron). In such case we can restore the RL(R) dimensions of the internal pions from the electron (positron) dimensions. When applied for kaon structures  $K^+$  and  $K^-$ , however, the factor  $k_S$  appears approximately valid. The reason is that the kaon is made of straight FOHS's, while the muon and pion are made of SOHS's. A straight FOHS could not be submitted to a large twisting without be converted to a SOHS. But if the kaon is not twisted like the internal pions, then it will have a slightly larger envelope radius, that means a slightly larger envelope volume for a single coil. Then we arrive to the following **conclusion**:

- **When applying the factor  $k_S$  for kaon structures  $K^+$  and  $K^-$ , we will get little bit larger value of the calculated destruction energy of their RL(T).**

Having in mind the above rule, we may apply a proper correction.

One approximative method for calculation of the RL(T) destruction energy for kaon structures, was given in §6.9.3.1 by using the experimental values of 1.7778 GeV and 1.44 GeV and the calculated value for the kaon length.

In the following two paragraphs other two methods will be used and the results will be compared.

#### 6.9.4.3.1 Aproximative calculations by using the CL asymmetrical factor

The radius change due to the twisting is relatively small. So we may use the volume dependence of the destruction energy. For a small range of volume change we may replace the two antipressure curves, given by Eqs. (6.12) and (6.1) (plotted in Fig. 6.9) with one curve. The simple curve  $y = \frac{1}{V}a$ , is pretty close to the both original curves, if a proper normalization is applied, by the selection of the constant  $a$ . The comparison between the simple curve and the original one for +RL, for a small range of volume change is shown in Fig. (6.13). f

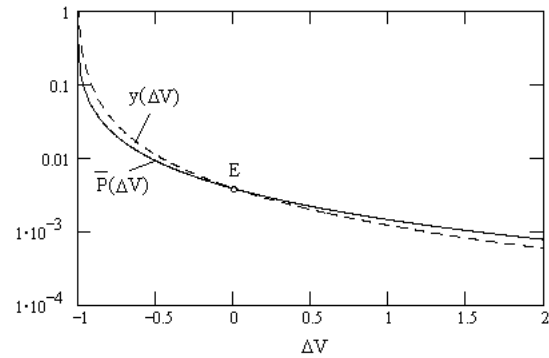


Fig 6.13

The volume change is referenced to the equilibrium point E, corresponding to the antipressure equivalent point between +RL(R) and -RL(T), satisfied for the volume ratio of  $K_S^2$ . In such case the destruction energy for the equivalent point E is the energy of the W bosons.

$$E_{D(R)} = E_{W^+} = E_{W^-} = 80.396 \text{ [GeV]} \quad (6.35.a)$$

The constant  $a$  is properly selected in order the fitted curve  $y$  to intercept the real curve of RL(R) at point E. Using the simple curve  $y(\Delta V)$ , the destruction energy at the reference point, the volume change determined by  $K_S$  and applying the asymmetrical factor  $a_{\text{sym}}$  in proper way, the destruction energies for both RL(T) structures of the kaon are obtained. They are annotated as  $E^+_{D(T)}$  and  $E^-_{D(T)}$ , and shown in Table 6.6. together with the experimental data. The index  $T$  stands for the twisted option of RL. The combined factor, given in the

table shows the correct use of the factors  $K_S$  and  $a_{sym}$ . In other words,  $E^+_{D(T)}$  and  $E^-_{D(T)}$  are destruction energy respectively for the RL structures of  $K^+$  and  $K^-$ . The

Table 6.6

Reaction	Combined factor	Calculated [GeV]	Experimental [GeV]	Note
$E^+_{D(T)}$	$\frac{1}{k_S^2} a_{sym}^2$	119.46		
$E^-_{D(T)}$	$k_S^2 \frac{1}{a_{sym}^2}$	94.34	91.187	Z boson

Comparing the values from Table 6.6 with the previously calculated, from Table 6.5, we see, that they are pretty close. For the values, shown in Table 6.6, the shrink factor  $k_S$  is used explicitly, while in Table 6.5 it is involved but implicitly. The deviation of the calculated value for +RL(T), from the experimental one, according to BSM is a result of :

- smaller twisting factor for the kaon RL(T) in comparison to the muon
- anisotropy of the RL(T) stiffness along the two axes - the radial and the tangential one.

The both features are taken into account in the next paragraph

### 6.9.4.3.2 Calculation of RL(T) destruction energy by using the twisted angle

Fig. 6.14 illustrates the shape, obtained by the radial stripe of RL(T), after the twisting.

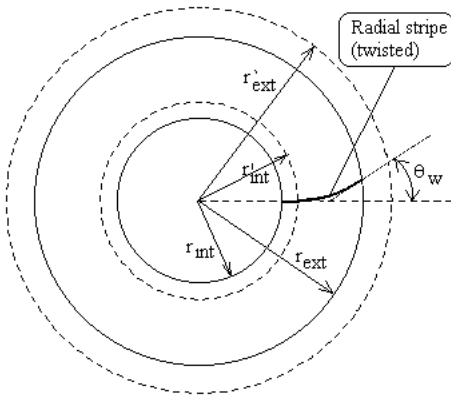


Fig. 6.14

The external and internal radii of the layer are denoted by prime. The following relations are valid;  $r_{ext}/r'_{ext} = r_{int}/r'_{int} = k_S$   $r_{int} = 0.5r_{ext}$

The degree of the twisting is determined by the balance of IG forces. It is evident that every layer get a similar shrink, due to the twisting, and the tangential angle of the tangent line in the point of radial stripe at max layer radius, should be one and a same for any layer. This is the angle  $\theta_w$ , shown in the figure. For the most external layer of +RL, this is the tangent angle, where the twisted radial stripe is connected to the helical boundary. So this is a characteristic angle of the twisted RL(T) structure, according to BSM. We will show, that:

- The characteristic angle of the twisted RL(T) structure corresponds to the effective mixing parameter  $\sin^2 q_w$  used in the electroweak theory

We will use the effective mixing parameter for “leptons”, to which category the electron belongs. We may rely on this parameter, as it is experimentally determined, from on-resonance observations at LEP (Large Electron Positron collider at CERN, Switzerland) and SLC (Stanford Linear Collider, USA). The best averaged value for this parameter, according to G. Degrassi et al. (1997) is:

$$\sin^2 \theta_{eff}^{lept} = 0.23165 \pm 0.00024 \quad \theta_{eff}^{lept} = 28.762 \text{ deg} \quad (6.36)$$

So we have to prove, that:

$$\theta_w = 28.762 \text{ deg} \quad (6.37)$$

In order to prove the statement made above, we have to know, the shape of the curved radial stripe after the twisting. This could be found, by the analysis of the sectional stiffness. Knowing that the radial distances between RL cells are equal, while the tangential are changed linearly, and having in mind the IG law, it is not difficult to guess, that the shape of the curved radial stripe is parabolic. The correctness of this assumption will become apparent from the final result.

We may express the tangential stiffness by the inverse cubic root of the tangential force, in a similar way as for the RL(R). The graphic plot of

the stiffness, expressed in this way is shown in Fig. 6.15

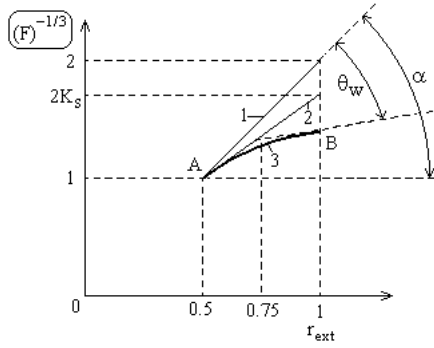


Fig. 6.15

Tangential force for parabolic shape of the radial stripe (curve 3) for RL(T)

The inverse cubic expression of the tangential force with parabolic shape of the RL(T) is shown as curve 3. The line 1 is for untwisted RL(R), while the line 2, for twisted but with linear dependence instead of parabolic. The angle  $\theta_w$  is the characteristic angle, mentioned above.

The horizontal axis corresponds to the smaller radius of FOHS. The values are normalised to  $r_{ext}$  of a complete layer. The curve 3 could be used for +RL(T), possessing complete layers (between 0.5 and 1 of  $r_{ext}$ ) and for -RL(T), that is not complete layer. In the second case, having in mind the ratio  $r_p/r_e = 2/3$ , the curve 3 between 0.5 and 0.75  $r_{ext}$  should be used.

In order to obtain the expression for curve 3, we use a parabola given by equation:  $y = x^2 \tan(\theta_w)$  (6.38)

where  $x$  is the running parameter

To obtain to equation of curve 3, the parabola has to be properly rotated and translated. The point of the rotation is at the origin of the parabola, while the rotation angle is  $(\alpha - \theta_w)$ . The rotated curve, then is translated in order, the origin to obtain the coordinates of p.A (see Fig 6.15). One may note, that the drawing plane of Fig. 6.15 is isotropic, i. e. the scale ratio between vertical and horizontal axes is 2:1. But the curved radial stripe, also obtain a similar isotropic scale, because: The scale of the radial axes is linear (the unit cell length is a constant), while the scale of the tangential axes (normal at radial one) is quadratic (the unit cell length in this di-

rection changes linearly from 1 to 2 for a radius range from 0.5 to 1  $r_{ext}$ ). In such conditions, the used approach for the rotation and translation of the parabola is correct. Using the rotational and translational transformation, according to the above consideration we obtain:

$$Y = 1 - [x \sin(\alpha) + x^2 \tan(\theta) \cos(\alpha)] \quad (6.39)$$

$$X = [x \cos(\alpha) - x^2 \tan(\theta) \sin(\alpha)] + 0.5 \quad (6.40)$$

where:  $X$  and  $Y$  are the new coordinates, that match the axes scale of the  $(F)^{-1/3}$  plot.

The angle  $\alpha$  is directly determined by the plot of line 1.

$$\alpha = \text{atanh}(0.5) = 63.435 \text{ deg}$$

$X$  and  $Y$  coordinates for number of points in the range of  $0 < x < 0.5$  are calculated and fitted to simple equation. The obtained equation represent directly the inverse cubic root of the tangential force of the curved radial stripe:

$$(F)^{-1/3} = \left(a + \frac{b}{x}\right)^2 \quad (6.41)$$

where:  $a$ ,  $b$  are coefficients, depending of  $\theta_w$

The change of the tangential forces from the twisting gives the stiffness change. The change of stiffness is proportional to the change of the antipressure, that according to Eq. (6.8) is proportional to the destruction energy. We may express the change of the tangential forces for +RL(T) and -RL(T) in own system, and compare the result for +RL(R) and -RL(R) also in own system. In this approach we do not need to use the CL asymmetrical factor. In such case, the area below the curve 3 and horizontal axis corresponds to the area stiffness referenced to the RL cell dimensions. The stiffness dependence of the twisting angle  $\theta_w$ , is indirectly determined by the coefficients  $a$  and  $b$  of Eq. (6.40). Having in mind, that the length of FOHS is not changed by the twisting, we may use the antipressure parameter instead of area stiffness. Later we will operate with ratio between antipressures. In the same time the antipressure is considered normalised to its maximum radial value at  $r_{int}$  (because the tangential force is normalized to  $r_{int}$ ). So for antipressure dependence of  $\theta_w$  we get:

$$\bar{P}_T^+(\theta_w) = \int_{0.5}^1 \left\{ \left(a + \frac{b}{x}\right)^2 \right\}^{-3} dx \quad \text{for +RL(T)} \quad (6.42)$$

$$\bar{P}_T^-(\theta_w) = \int_{0.5}^{0.75} \left\{ \left( a + \frac{b}{x} \right)^2 \right\}^{-3} dx \quad \text{for -RL(T)} \quad (6.43)$$

where: the dependence of a and b from  $\theta_w$  is given by the Eq. (6.41), (6.42), (6.43); the index T stands for twisted RL

Note: The integration shown in Eq. (6.42) and (6.43) is referenced to the unit cell in a similar way, as the integration for RL(R), given by Eq. (6.17) and (6.21). This gives us the possibility to expect an accurate result from the ratio between the twisted and radial RL. For the case of +RL, we may also, use the ratio for one layer, but it will be valid for all layers., and consequently for all +RL structure. Then using such ratio and referencing the energy scale to the destruction energy for untwisted RL(R) we get:

$$E^+_{D(T)} = 80.396 \frac{(\bar{P}_T^+(\theta_w))}{\bar{P}_0^+} \quad \text{for +RL(T)} \quad (6.44)$$

$$E^-_{D(T)} = 80.396 \frac{(\bar{P}_T^-(\theta_w))}{\bar{P}^-} \quad \text{for -RL(T)} \quad (6.45)$$

The Table 6.7 shows the calculated results for the destruction energies of both type RL(T), for two values of  $\theta_w$ . In the same table, the values calculated by the previous methods, and the experimental values are given

Table 6.7

Parameter	$\theta_w$ 28.72 [deg]	$\theta_w$ 26 [deg]	Ref. to Table 6.5 [GeV]	Ref to Table 6.6 [GeV]	Experim. value [GeV]	Note
$E^+_{D(T)}$	107.19	104.86	119.26	119.46		
$E^-_{D(T)}$	92.03	91.115	96.6	94.34	91.187	Z boson

The a and b coefficients for both value of  $\theta_w$  are:

for  $\theta_w = 28.72$  deg  $a = 1.43095$   $b = -0.21401$   
 for  $\theta_w = 26$  deg  $a = 1.454949$   $b = -0.227265$

We see, that the closest value of  $E^-_{D(T)}$  to the experimentally measured one is at  $\theta_w = 26$  deg. The value is:

$$E^+_{D(T)} = 104.86 \text{ GeV} \quad (6.46)$$

The value obtained by this method should be more correct, that the values determined by the previously two methods. The previous approximative methods do not take into account the different

shrink factor for the charged kaons, and the stiffness anisotropy between the radial and axial directions of the RL structure.

Looking for a possible observed resonance at 104.86 GeV, we really find an evidence of such. A strong evidence for resonance at 105 GeV is found in the CERN document titled “ Search for Higgs bosons: Preliminary combined results using EP data collected at energies up to 202 GeV” (CERN-EP-2000-055, April 25, 2000). The document is posted in Internet. Fig .6.16 shows the resonance as “reconstruction Mass  $m_H$  [GeV/c<sup>2</sup>] (corresponding to Fig. 4 of the document).

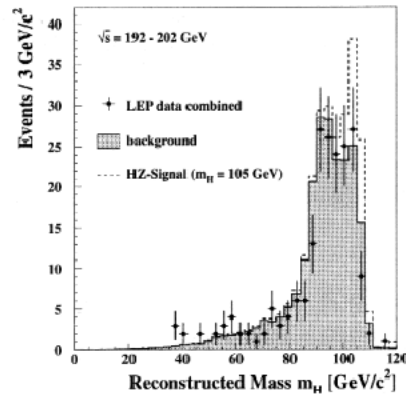


Fig. 6.16

(from technical document, published by CERN, 2000)

Paper text: “Fig. 4 : LEP-combined distribution of the reconstructed SM Higgs boson mass...The figure displays the data (dots with error bars), the predicted SM background (shaded histogram) and the prediction for a Higgs boson of 105 GeV/c<sup>2</sup> mass (dashed histogram)....”

Another indication of resonance at 105 GeV is found from the paper presented by W. M. Yao at

FERMILABAB -Conf-99/100-E, also posted in Internet. .

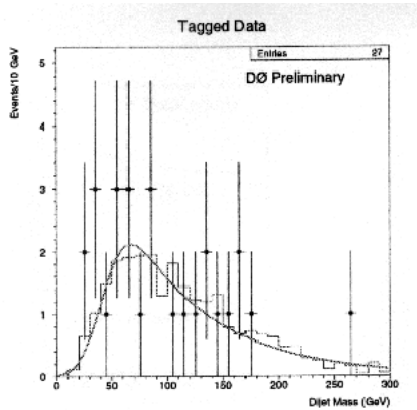


Fig. 6.17

Paper text: “Fig.1. The measured two-jets mass distribution along with background ...”

The paper shows a plot of the parameter “two jet mass distribution”, in which slight evidence of the 105 GeV resonance is apparent. The statistical noise is large due to the small number of obtained events. Fig. 6.17 shows the plot of the above mentioned parameter (corresponding to the Fig. 1. (right) of the paper)

The resonance at 105 GeV may not appear so well defined as the 91.115 GeV resonance. The latter is from a destruction of only one RL(T) layer, while the first one is from many layers of the same type. The stiffness of interconnections between the same type of layers, even, when they are twisted is much weaker, than the stiffness of a single layer. Then quite high probability exists, the +RL(T) structure to be separated in number of layers. In such case their destruction jets could have different spatial positions and directions. This does not match to the accepted criterion for identification of “boson mass” in the experiments, provided in the particle colliders. Additionally, the central negative core could catch part of positive internal RL(T) layers, forming a different jet. This case will be similar as the observed 3-rd track of high energy e+e- collision, where the third track is from some layers of +RL(T), catch the central negative core (see Fig. 6.6 (courtesy of J. Z. Bay et al, (1996)).

The derived analytical method shows good consistency between calculated and experimental

values, and correct dependence of the destruction energy from the twisting angle  $\theta_w$ . One additional experimental proof for the concept is the observed asymmetry of Z boson “mass”. It is known as forward-backward charge asymmetry” (see Abreu, (1994)). More accurately this is asymmetry between the right and left wing of the resonance energy. The  $w^\pm$  boson “masses” does not possess such asymmetry. Experimental data about Z boson “mass” asymmetry, referenced as forward-backward charge asymmetry is shown in Fig. 6.18 (Abreu, (1994)).

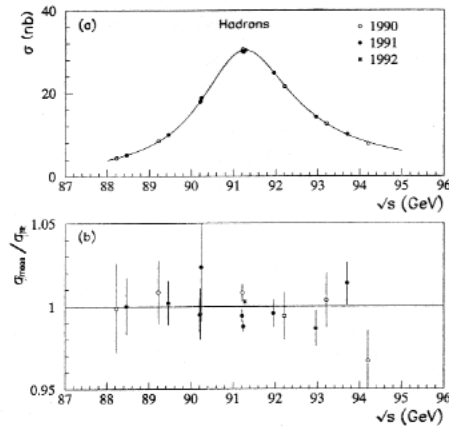


Fig. 6.18

BSM interpretation: The asymmetry between left and right wing

Source paper text: Hadronic cross section from 1990, 1991 and 1992 data. In (a) the data are shown together with the result of 5-parameter fit. Plot (b) shows the ratio of the measurements to the best fit value

The BSM explanation of the asymmetry is the following: The destruction energy of RL(T) in function of  $\theta_w$  exhibits a definite trend. The twisting process involving large IG energies, may exhibit small aperiodic oscillations of the twisting angle  $\theta_w$ . Such oscillations could be centred around the calculated value  $\theta_w = 26 \text{ deg}$  (for  $K^-$  and  $K^+$ ). The destruction process may be initiated during these oscillations. The variation of  $\theta_w$  means variation of the volume of FOHS, that defines the initial volume V1 in the integral of eq. (6.8). Consequently the variation of  $\theta_w$  leads to variation of the destruction energy. Then the observed resonance will be a weighted function of number of individual destructions for a gaussian type of deviations centred around 26 deg. The positive de-

viations of  $\theta_w$  will correspond to larger twisting, and consequently larger destruction energy. This explains, why the right hand wing of the Z boson “mass” is higher than the left hand one.

*Conclusions:*

- **The angle  $\theta_w$  is a characteristic angle, characterizing the degree of twisting of the full thickness layer of RL(T).**
- **The value  $\theta_w = \theta_{eff}^{lept} = 28.762$ , used in the electroweak theory corresponds to the degree of twisting obtained by a SOHS (as muon, positron, proton external shell). At this angle the IG forces balance equation (2.8) is fulfilled for CL space environment.**
- **The characteristic angle for a straight FOHS (as the charged kaon) is little bit lower, than the value of  $\theta_{eff}^{lept}$ . its calculated value is about 26 deg**
- **The characteristic angle is one and a same for positive and negative RL, but having in mind, that the latter one possesses “not full layer” thickness.**

#### 6.9.4.4 Relation between Fermi coupling constant and the equivalent IG energy corresponding to the twisting

The Fermi coupling constant is another basic parameter of the electroweak theory, that is experimentally determined. It was discussed in 6.4.4.5 in connection with the muon lifetime, related to the process of pion-muon conversion. The common process between this conversion and the  $\beta$  nuclear decay is the helical structure twisting (including the internal RL structures). In the case of the  $\beta$  decay the twisting affects all substructures of the nuclei. Now we will give an additional proof for the concept of pion-muon conversion and its relation to the twisting.

#### A. Twisting equivalent IG energy

The twisting equivalent energy,  $E_T$ , is an energy difference between the destruction energy of RL(T) and RL(R), for structures of same type handedness.

$$E_T = E_{D(T)} - E_{D(R)} \quad \text{GeV}$$

The energy  $E_{D(R)}$  was discussed in §6.9.4.2 as equal to the  $W^\pm$  mass-equivalent energy (see Eq.

(6.35.a). Then the twisting equivalent energy for the  $K^+$  and  $K^-$ , according to the data, shown in Table 6.7, is respectively:

$$E_T^+ = 104.86 - 80.396 = 24.46 \quad \text{GeV} \quad \text{for } K^+ \quad (6.47)$$

$$E_T^- = 91.187 - 80.396 = 10.79 \quad \text{GeV} \quad \text{for } K^- \quad (6.48)$$

*Note:* The calculations are for single structures only, i.e. the negative structure does not contain internal positive one. According to BSM, this corresponds to the experimental conditions for the bosons mass estimation.

#### B. Estimation of the twisting equivalent IG energy by the Fermi constant

According to R. Feynman and M. Gell-Mann (1958), the Fermi coupling constant is  $(1.01 \pm 0.01) \times 10^{-5}/m_p^2$ , where  $m_p$  is the proton mass. Substituting  $m_p = 0.9383 \text{ GeV}$ , we get the value  $1.1358 \times 10^{-5} [\text{GeV}]^{-2}$

The current accepted value of the Fermi coupling constant according to NIST data is:

$$G_F = 1.16639 \times 10^{-5} \quad [\text{GeV}]^{-2} \quad (6.49)$$

Expressing in units of GeV we get:

$$E_{T(p)} = [1.16639 \times 10^{-5}]^{-1/2} = 292.8 \quad \text{GeV} \quad (6.50)$$

where:  $E_{T(p)}$  - is the equivalent IG twisting energy for neutron-proton conversion

The NIST value is determined by the muon lifetime, that according to the BSM is related to the twisting in the pion-muon conversion. However it is still normalised to  $m_p^2$ . In other words, it is related to the average twisting energy of the pion muon conversion, but normalised to  $m_p^2$ . The average twisting energy takes into account the energy estimation in confined process, that was described in §. When referenced to the newtonian mass it implicitly takes into account the relation between the asymmetrical factor  $a_{sym}$  and the newtonian mass correction  $k_m$ , given by Eq. (6.35). **When estimated by the destruction energy, however, the average value of  $E_T^+$  and  $E_T^-$  should be used.**

The energy  $E_{T(p)}$ , given by Eq. (6.50) is implicitly normalized to  $m_p^2$ . Let to renormalise it to the muon, by proper use of the mass ratio  $m_p/m_\mu = 0.9383/0.1057$ . Then we get the average equivalent IG twisting energy for pion-muon conversion, mentioned above.

$$E_{T(\mu)} = \left[ G_F \frac{m_p^2}{m_\mu^2} \right]^{-1/2} = 32.98 \quad [\text{GeV}] \quad (6.51)$$

According to the above mentioned considerations, the same energy could be estimated by the average destruction energies, given by Eq. (6.47) and (6.48):

$$E_{T(\mu)} = E_T^+ + E_T^- = \frac{24.46 + 10.79}{2} = 35.25 \text{ [GeV]} \quad (6.52)$$

The results (6.51) and (6.52) are pretty close. The small difference could be contributed to the use the  $k_G$  factor for the kaon twisting, while it is accurately valid for the twisting from pion to muon conversion. In any case, the results are close enough, in order to validate the correctness of the pion-muon conversion mechanism and the relation between the muon lifetime and the equivalent twisting IG energy. The latter one is directly related to the Fermi coupling constant.

The equivalent IG twisting energy of 292.8 GeV, given by Eq. (6.49) is implicitly referenced to the proton. It is equal of the sum from individual twisting energies of all the substructures. The budget of this energy will be cross calculated and compared in §...

#### Summary:

- **The Fermi coupling constant is estimation of the equivalent IG twisting energy**
- **The nuclear  $\beta$  decay, the pion - muon decay, and the neutral kaon - charge kaons decay are related with common phenomena - twisting of their FOHS's.**
- **The twisting of the FOHS does not change its length**

### 6.10 Physical explanation of the Neutonian gravitation and inertia of the elementary particles as interactions between IG(CP) forces of the RL(T) structures from one side and the CL space from the other.

#### 6.10.1 Relation between RL state and IG forces balance

From the provided analysis and the interpretation of the experimental data, we found that the destruction energies of +RL(R) and -RL(R) are balanced for radius ratio  $r_e/r_p = 2/3$ . When the FOHS is twisted, the radius ratio is preserved, but the destruction energies of +RL(T) and -RL(T) are different. The criterion for a stable helical structure requires IG forces balance according to Eq. (2.8).

In this equation, however, additional forces are included - the opposing bending forces of the helical envelope. In CL space the interaction forces between RL(TP) and CL node (TP) forces are also included, but they are comparatively small and could be ignored. We may accept that:

- The degree of twisting is determined by the balance of all IG forces according to Eq. (2.8).
- The IG forces of stable helical structures in CL space are not detectable in the normal interaction processes

The first conclusion means, that the free FOHS get twisting until the balance eq. (2.8) is fulfilled. The direct proof of this conclusion is difficult, but it becomes evident, from the course of the BSM.

**The second conclusion is valid for normal processes of interaction**, in which the stable helical structure does not change its parameters: twisting and shape. This exclude the high energy interaction as the particle destruction and high energy scattering (including Babha and Moller scattering). **The normal processes of interactions include:**

- Neutonian gravitational mass
- Neutonian inertia
- Electric field
- Magnetic field

#### 6.10.2 Neutonian gravitational and inertial mass of a helical structure

Let to analyse the possible interactions between the IG(CP) forces of a helical structure and the nodes of CL space. For these purpose, the following two cases, will be considered.

Case A: a single particle formed of external and internal FOHS's is away from any other helical structure or gravitational filed

Case B: two identical particles formed of FOHS's are in close distance, but away from external gravitational field.

A typical example for the case A, is the single electron, away from other particles possessing neutonian mass. Let to consider in first, that the electron is in rest in CL space. The both RL(T) structures carry an enormous intrinsic mass, but their IG(CP) forces are accurately balanced due to the symmetry. **So they do not interact with CL**

**space nodes and appears as hidden.** The IG(TP) forces, however, are not balanced (due to the prism to prism interaction, discussed in Chapter 2), and they contribute to the E field of CL space, characterised by an unit charge. **Now let to consider, that the same particle is in motion** with not relativistic velocity. It now possesses a kinetic energy. **The universal energy conservation principle requires, that the energy balance in the IG system should be preserved.** The electrical charge, contributed by the IG(TP) is a same, so the IG(TP) interaction with the CL space is a constant. The only left option, for restoring the energy balance is a possible interaction between IG(CP) forces and the nodes of the CL space. This means, that IG(CP) field for the moving structure is not any more hidden for the CL space. The generated disturbance from the twisted IG(CP) of the most external RL layer, is involved in this type of interaction. **This effect is manifested as a Neutonian inertia of the helical structure.**

**In case B,** we have the same two particles but in close distance. In this case, some influence could appear between the IG(CP) of the structures so the accurate balance between the IG(CP) forces of the structure and the CL space should be disturbed. In case of two shell structure (internal positive and external negative) possessing RL(T)'s, the major contribution for the disturbed balance is from the external shell. Due to the disturbed balance, a forces of attraction appears between the two particles, whose sum could be expressed by a common attraction force. The propagation media for these forces is the CL space between them. It becomes apparent, that the common attraction force is propagated by the (CP) of the forming the CL nodes. We may express the common force as a summation of the individual forces from every point of the first particle, exhibiting IG interaction from the second one within subtended angle. If the distance between the two particle changes, the subtended spatial angle also changes with the inverse square root of the distance. In this interaction the CL space nodes are involved, and they are always outside of the FOHS volume. This is completely consistent with the definition of the mass equation, valid for the neutonian mass. So we arrive to the conclusion, that the described above interaction is

a Neutonian gravitation, known as “universal gravitational law”.

We see, that in the Neutonian gravitation, the CL nodes are directly involved, however, their intrinsic masses are hidden. The neutonian mass is proportional to the static pressure, while the latter has some connection to the IG forces.

#### *Conclusions:*

- **The Neutonian gravitation is a result of disturbed balance between the IG(CP) of two close helical structures, in CL space environment. its manifestation is the universal gravitational law.**
- **The Neutonian gravitation depends only of the volume of external helical shell of FOHS**

The second conclusion provides explanation of the **effect of the hidden neutonian mass.** This effect appears for the internal positron, and the positive internal structure of the negative muon and pion.

#### **6.10.3 Radial gap between different type of helical structures.**

Let to consider again the electron system. For proper oscillation of the system, two radial gaps are needed:

- between the -RL(T) and the positron helical structure
- between the central negative core and the internal radius of the most internal +RL layer.

It is experimentally verified, that electrons and positrons may obtain a strong polarization after striking a plane surface under angle. The strong polarisation, according to BSM, is indication for the existence of the mentioned above gaps.

The mechanisms assuring the both gaps are different, because the +RL and -RL structures are different.

##### A. Internal gap of +RL(T) structure

The internal gap of +RL(R) structure is determined by two factors:

- finite length of the prism
- an anisotropy of IG propagation through the prism

The second factor is intrinsic feature of the intrinsic matter, manifested in the prisms formation. It means, that the axial prism vector of IG

force is larger, than the radial one. (It is to be discussed in the last Chapter of BSM).

The finite length of the prisms means a finite number of layers for +RL structure. In the following analysis it is shown, that the number of layers could be determined if we know the gap between the prisms in CL space. In Chapter 3, the node distance along xyz axes is calculated as  $d_{nb} = 1.1 \times 10^{-20}$  m. This is in CL unit length scale. Applying the correction factor of 0.8165 for a positive prism (lefthanded assumed) we get a value of  $0.8981 \text{E-}20$  m. The CL node distance along abcd axes is approximately half of xyz distance, so it is  $0.449 \text{E-}20$  m. The unknown parameter for CL space is the “gap to node distance ratio” for abcd axes. (The gap is between the neighbouring prisms, that are of different type). Let to assume, for example, that the gap is equal to the sum of right and left handed prisms length. When referenced to CL scale unit, it is equal to  $2 \times 0.8165 = 1.633$ . Now referencing to the positive prism scale it is  $1.633 \times 0.8981 \times 10^{-20} = 1.4665 \times 10^{-20}$  m. This value is half of the CL node distance (along abcd). Now expressing the CL node distance by the positive prism scale we obtain:  $2(L_L + L_R) = 2(L_L + 1.5L_L) = 5L_L$ . So we get:  $L_L = 1.4665 \times 10^{-20} / 5 = 0.2933 \times 10^{-20}$  m. Then the minimal node distance in the +RL(R) layer is twice this value or:  $0.5866 \times 10^{-20}$  m. Theoretically the smaller internal radius of the most internal layer is equal to the minimal node distance. This put the **theoretical limit of the internal hole radius** to be also  $0.5866 \times 10^{-20}$  m. From the other side, knowing the positron small radius  $r_p$ , and applying the rule of the half radius layer thickness we may express the hole radius by the equation:

$$r_{hole} = r_p \left[ 1 - \sum_{i=1}^l \frac{1}{2^i} \right] \quad (6.52)$$

where:  $i = 1$  in this equation corresponds to the most external layer of +RL(R).

The bar plot of Eq. (6.52)  $15 < l < 22$  is shown in Fig. 6.19. In the same plot the theoretical limit of the radius is shown as a dash line.

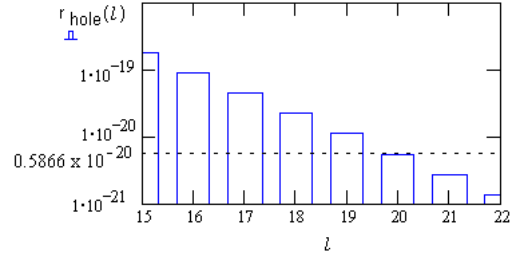


Fig. 6.19

The theoretical limit coincides with the value 0.5866, with amassing accuracy for number of layers equal to 20.

Note: The obtained number of layer is dependent of CL node gap, but not in large range. It also does not take into account the IG anisotropy, mentioned above. So in the real case, the number of layers may be smaller, assuring larger hole radius.

Radial node distance affected by the finite length to radius ratio of the prism.

Due to the finite thickness (diameter) of the prisms, and the radial dependence of the tangential stiffness within one layer, the radial scale exhibits a small deviation from the linearity. This is illustrated by Fig. 6.20, where: **a.** shows RL nodes in a radial section near the small layer radius; **b.** shows

a similar section near the large radius; **c.** shows the enlarge scale of nodes in case a. .

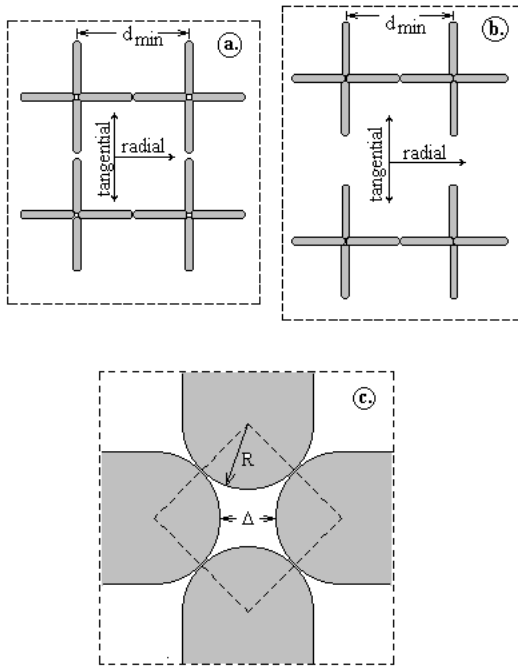


Fig. 6.20

Radial displacement due to a finite prism thickness

It is obvious, that the deviation from linearity is a function of L/R ratio of the prism. (In Chapter 12 it will be shown, that this ratio is a constant for all prisms belonging to one galaxy, but may have slight variation between the prisms of different gal-axes).

The slight non linear radial scale leads to slight increase of the central (“trapping”) hole. Knowing the radius  $r_p$  and the number of layers, the radius of the hole could be calculated for a chosen L/R ratio. Approximate calculations for  $L/R = 12$  and number of +RL(R) layers = 20, leads to a result,  $r_{hole} \approx 1.6\%$  of  $r_p$ .

### Radial gaps in combined helical structures with RL(T).

After the twisting, the radial gaps of the combined helical structures is increased. This conclusion follows from the following features, demonstrated by the experimental data:

- the strong polarization of the electron and the free positron after striking a plane under angle
- the difference in the two main decay reactions of  $K_S^0$  with highest fraction ( $\Gamma_i/\Gamma$ ):

The first feature is well known by the experiments. The second feature is related to the reactions

The second feature is related to the decay reactions:

Mode	Fraction ( $\Gamma_i/\Gamma$ )
$K_S^0 \rightarrow \pi^+\pi^-$	68.61 %

(6.53)

$K_S^0 \rightarrow \pi^0\pi^0$	31.39 %
--------------------------------	---------

(6.54)

In the reaction (6.54) the both pions are pair of separated untwisted structures - one negative and one positive with internal structures respectively -RL(R) and +RL(R). Consequently they have been untwisted before and during the time of separation. The difference in the fraction parameter for the both reaction could be explained by the differences in the radial gaps. Despite the fact, that the end product of the reaction (6.53) are charged pions, the fraction parameter for this reaction is larger. This means, that the separation in this case is easier. This could be contributed to a larger radial gap. This gap corresponds to the gap between the internal radius of -RL(T) and external radius of +RL(T). In case of the electron system and the negative muon, this gaps is even little bit larger, due to the additional twisting (because they are SOHS’s).

There are **two additional features that may lead to increased gap between the electron shell and the positron:**

- a) the structural difference of +RL from -RL:
- b) the reduced layer thickness of -RL

The feature a) is characterized with:

- the intrinsic matter of +RL(T) structure is in radial range of  $0 \approx r_{hole} < r < r_p$
- the intrinsic matter of -RL(T) is in the radial range of  $r_p < r < r_e$

In the first case the radial size could be kept more compact due to additional diametrical IG forces. In the second one, such forces are absent due to the larger hole.

The feature b) means, that the tangential stiffness of

-RL changes in smaller range in comparison to the tangential stiffness of +RL. Consequently the centre of mass of the IG matter density in -RL(T) will be displaced toward the larger layer radius in comparison to the +RL(T). This assures additional gap

increase between the electron shell and the positron.

*We may summarise:*

- **The radial gaps between the substructures of the combined negative helical structure assures conditions for oscillations without internal energy loss**
- **The central positions of the oscillating structures are kept by the radial configuration of the IG field**
- **The oscillation motion is frictionless**
- **The radial gaps for the electron system and the negative muon are equal. (The same rule is valid for the free positron and the positive muon).**

#### 6.10.4 Real newtonian mass of the kaon

Kaon has been one big enigma in the particle physics. The BSM concept succeeded to explain most of the features of the kaon until the discovering of its last puzzle parameter: the mass of the kaon structure in all of its modifications ( $K_L^0$ ,  $K_S^0$ ,  $K^+$ ,  $K^-$ ) does not fit to the model. According to the model the internal kaon should have the mass of mass of  $K_L^0$ , but the experimentally determined mass did not fit. If it is multiplied by the factor of 11 it fits excellent when using the mass equation for calculating the masses of the proton (neutron), eta particle, antiproton/proton stopping power,  $w^\pm$  bosons and Z boson. Finally it was found by the analysis of the pulsars, that **all the kaon masses are experimentally determined with large error due to neglecting the trust force from its jet.**

Pulsars theory, presented in Chapter 12, shows that the pulsar is a kaon nucleus, i. e. a huge bunches of aligned straight FOHSs (like the single kaon) possessing a super strong axial magnetic field and propulsion jet system of continuously destructed RL(T). Such nucleus is formed by crushed protons and neutrons in the star centre due to enormous gravitational pressure. The process starts in the instability region of H-R diagram and is again activated at the phase of star dying.

The same conditions valid for the pulsar (with one jet) are valid for a single kaon. The destruction of its internal RL structures starts after it is released from a cut proton (neutron). The destruction is in form of single jet providing strong

thrust force of the structure (as a rocket). The straight shape of the structure and the active linear momentum provides conditions for a strong local magnetic field with axial alignment. This field influences the spatial angle of the jet fuse and finally the fuse cone volume. The released RL nodes has a limited lifetime and they are converted to folded CL nodes. The pulsar theory shows that the **conversion rate per unit CL space volume is a constant parameter** determined from the CL space ( $\Lambda/V = \text{const}$ , see §12.B.6.4.3). It also shows, that the cone angle and the conic volume depend of the magnetic field, but the latter is continuously decreasing during to pulsars life (proportional to decreasing nuclear matter). For this reason it mimics successfully a passive body with initial birth velocity. The same conditions are valid for the single kaon. The burning part of single kaon is illustrated in Fig. 6.21.

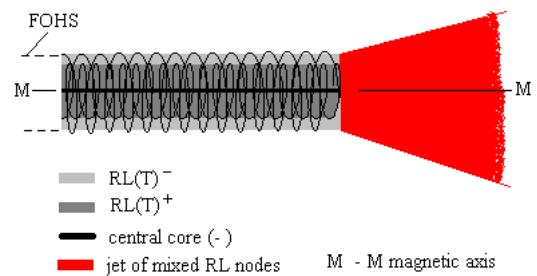


Fig. 6.21  
Burning end of kaon

It is apparent, that:

**If the kaon is considered as a passive particle with a finite lifetime its rest mass will be significantly overestimated.**

The kaon jet may provide not only incorrect experimental masses of kaons's structure modifications but also for the eta particle and short lived "antiproton" (that could possess a cut kaon), (see §6.12.2.4).

Question: Why the experimental masses of pions and muons appear correctly?

Answer: Both particle possess second order helicity. In the process of RL(T) destruction the debit of released RL nodes depends of the following three parameters: linear velocity, spin rate and angle between the jet and structure axis. Then the

peripheral part of the high velocity jet containing packet RL(T) structure may reach the light velocity but the flow debit to be below the parameter  $\Lambda/V = \text{const}$ . In such conditions a confined motion is preformed, allowing to detect a correct newtonian mass. For the muon, the angle between the jet and the structure axis is close to 90 deg and the conditions for confined motion are better. So its lifetime (structure burn time) is about two order larger in comparison to the pion. The conditions for axial magnetic field are also quite low.

**6.11. Common characterization parameters of the proton, neutron and proton.**

The proton, the neutron and the proton are distinguished only by the external shape and the degree of twisting of their substructures. If disregarding their common substructure, these three particles are closed loops, but with different shape. Let to use the term “**proton core**” for the body of this loop. We may summarize:

- **The proton core is the body of the closed loop, from which any one of the three particles, proton, neutron and proton, is formed.**
- **Referencing to the proton core is useful, when disregarding the internal substructure of the particle**
- **The length of the proton core is one and a same, for the mentioned three particles, while the shape is different.**

It is obvious, that the spatial configuration of the proton and neutron is defined by the following parameters:

- length of the proton core
- thickness of the proton core
- projection of the twisted shape on a plane
- external twisting angle of the loop

In the next paragraph we will see, that the determination of the dimensions of the proton core leads simultaneously to determination of some dimensional parameters of its substructure components.

**6.12 Proton**

**6.12.1 Structure and shape**

The proton is a complex helical structure composed of external structure  $TTH_1^3:+(-)$ , refer-

enced as external shell and internal structures of pions and a central kaon. The internal structure of the proton was shown in Fig.... The proton and neutron have the same internal structure, but distinguished only by the degree of twisting. The shape of the proton with exploded view of its external shell is shown in Fig. 6.22.

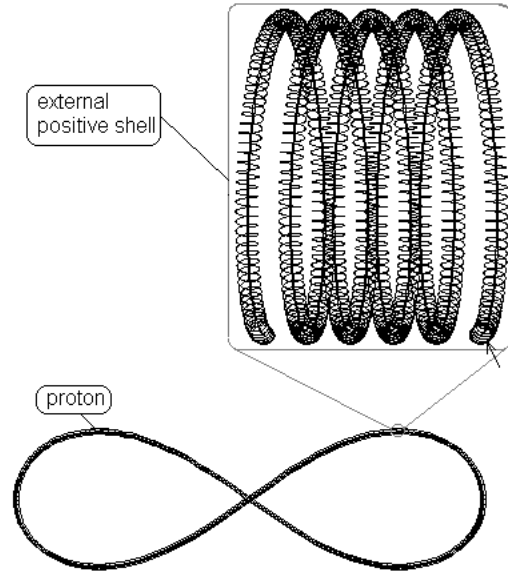


Fig. 6.22  
Proton

The central axis of folded proton core does not lie in a plane. For this reason we can call it a quasiplane. In order to use a simple mathematical expression, however, the quasiplane could be considered as a plane. The modelling of spring structure, possessing some degree of stiffness, shows that the most suitable mathematical function for the shape of the proton is the Hippopede curve. In polar coordinates this curve is given by Eq. (6.55), while in Decart coordinates - by Eq. (6.56)

$$r^2 = b^2(1 - a^2(\sin(\theta))^2) \tag{6.54.a}$$

$$(x^2 + y^2)^2 - b^2[x^2 + (1 - a^2)y^2] = 0 \tag{6.54.b}$$

The parameter a is related to the width to length ratio of the curve according to the equation:

$$\frac{1}{2\sqrt{a}} = \frac{W_p}{L_p} \tag{6.56}$$

where:  $W_p$  - is a full width of the curve  
 $L_p$  - is the full length of the curve

Based on a mechanical spring modelling (not presented here) the most suitable value of this factor is  $a = \sqrt{3}$ . The full length and width of the curve for this value is a characteristic parameter of the proton shape. They correspond to the dimensions of its internal core (more accurately the central kaon core), but will be further referenced as a proton length and width. The polar plot of Eq. (6.54.a) for the accepted value of  $a$  is shown in Fig. (6.23). The parameter  $b$  appears to be half of proton length.

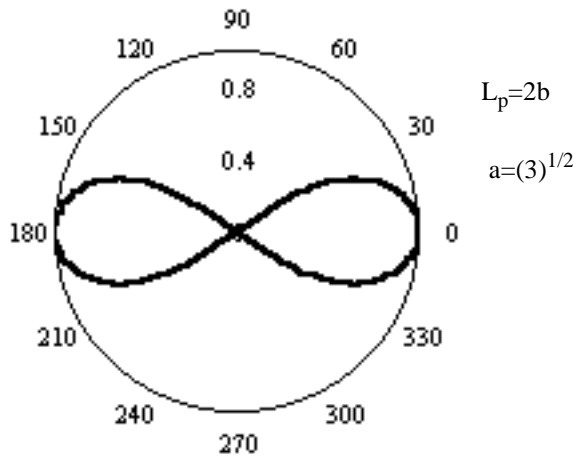


Fig. 6.23  
Proton shape by Hipped curve

We can call the two portions of the curve **proton clubs**. There are two important points in the plane of proton clubs, corresponding to maximal vertical width of the hipped curve. They are located on the horizontal axis at distance of **0.6455 b** from the curve centre. This point could be regarded as a centre of mass of the club. We can call this point **locuses**. The ratio between the length  $L_p$  and width  $L_w$  of the curve is:

$$W_p/L_p = 0.28867 \quad \text{for } a = \sqrt{3} \quad (6.56)$$

We shall adopt this factor of  $a$ , because it matches very well in all the equations in which the proton shape is involved.

The curvilinear length of the Hipped curve can be found by numerical integration in polar coordinates:

$$L_{pc} = 2L_p \int_0^{\theta_m} \sqrt{(1 - a^2(\sin\theta)^2) + \frac{a^4(\sin\theta)^2(\cos\theta)^2}{1 - a^2(\sin\theta)^2}} d\theta \quad (6.57)$$

where:  $L_{pc}$  - is the length of the curve, equal to the proton

core length;

$\theta_m = 0.19590657\pi$  - is the adjusted angle limit for the integration (in order to include the whole curve sector)

$L_p = 2b$  - is the proton length;

$b$  - is the outscribed radius

*Notice:* The upper limit of integral in the Eq. (6.57) depends of the  $a$  parameter and should be properly adjusted for any different value of  $a$  than  $\sqrt{3}$ .

By using the shape of Hipped curve, for  $a = \sqrt{3}$ , the proton dimensions can be completely determined if knowing the proton core length  $L_{pc}$ . This parameter was approximately determined, in Chapter 4, by using the equation of the CL space background temperature and its experimental estimate by the Cosmic Microwave Background. The latter phenomena has a different interpretation according to BSM.

### 6.12.2 Cross calculation method for accurate determination of the proton dimensions

#### 6.12.2.1 Accurate determination of the proton core length

In §6.9 it was proved that:

**The twisting of the FOHS does not change its length. In other words, the length of the FOHS of pion and muon are equal each other.**

Relying on this feature we can determine the  $L_{pc}$ , very accurately, by using the experimental data of some subatomic particles, obtained in result of proton destruction. For this purpose we will use the expressions for the mass equation, derived in Chapter 3. For correct application of the mass equation, we have to use correctly the shrink factor  $k_S$ , or its reciprocal  $k_R$ , and the mass correction factor of 2.25 for the positive helical structures. The true value of  $L_{pc}$  could be calculated by solving a system of mass equations. They should satisfy the following mass budgets, for which quite accurate experimental data exist

- Correct mass budget of the proton
- Correct mass budget of the eta particle
- Correct stopping power ratio between the antiproton and proton

Additional criteria used

- The number of second order turns of the internal pions should be an integer, because it is a curled toroid

- The calculated length of the proton core, should match closely the Cosmic Microwave Background experimental data

All of the masses, mentioned above are Neutronian masses.

**Note:** The mass of the Kaon determined in the particle experiments is overestimated because the thrust force from kaon jet (destruction of its RL structure) has not been discovered so far and not taken into account. (The existence of such jet is confirmed also by the pulsar theory provided in Chapter 12). So when using the mass equation for compound particle containing a stable kaon a proper correction factor should be used for the kaon. Fortunately this correction factor affects the mass budgets of the proton, the eta particle and the anti-proton/proton stopping power ratio in a different way. This provides the opportunity for pretty accurate determination of the mass correction factor of the stable kaon.

The parameter  $L_{pc}$  would be determined quite accurately, if we knew the helical radius of the internal pion and the second order step. Based on the provided so far analysis, we may choose a guessed value for the helical radius and test the equations of the mass budgets.

The helical radius is the radius of the projection of the pion SOHS in a plane normal to the proton core. In Chapter 3 it was mentioned, that during the phase of the crystallization, the internal cylindrical space closed by the external proton shell perhaps is formed of RL(R). (This is to be extensively discussed in the last Chapter of BSM). Then the equation (2.8) of IG forces balance could be satisfied for a value close to  $2/3$  of the radial distance between the external positive shell and the internal Kaon. So the corresponding internal pion radius,  $R_\pi$ , can be expressed as

$$R_\pi = \frac{2}{3}(R_c - r_p - k_R r_e) + k_R r_e \quad (6.57)$$

The length of FOHS in one turn of internal pion is:  $\sqrt{4\pi^2 R_\pi^2 + S_\pi^2}$  so the total length of its FOHS is:

$$n\sqrt{4\pi^2 R_\pi^2 + S_\pi^2} \quad (6.58)$$

where,  $s_\pi$  is the second order step of internal pion, and  $n$  is the number of its turns inside the proton.

One turn of muon is equivalent to the electron (positron). The number of turns in the muon are given by:

$$\frac{\mu_e}{\mu_\mu} = \frac{m_\mu}{m_e} = 206.76 = \frac{206.76 \text{ turns}}{1 \text{ turn}}$$

The FOHS length of one turn of the muon and the FOHS length of the electron (positron) are equal. Then the total length of the FOHS in the muon is

$$\left(\frac{\mu_e}{\mu_\mu}\right)^2 \sqrt{4\pi^2 R_c^2 + s_e^2} \quad (6.59)$$

Using the equality of the FOHS length of pion and muon, we equalise the expressions (6.58) and (6.59). Then solving for  $s_\pi$  we get:

$$s_\pi = \frac{1}{n} \left[ \left(\frac{\mu_e}{\mu_\mu}\right)^2 (4\pi^2 R_c^2 + s_e^2) - 4n^2 \pi^2 R_\pi^2 \right]^{1/2} \quad (6.60)$$

The total length of the pion as a SOHS inside the proton is a same as the proton core length  $L_{pc}$ . So  $L_{pc} = s_\pi n$  or

$$L_{pc} = \left[ \left(\frac{\mu_e}{\mu_\mu}\right)^2 (4\pi^2 R_c^2 + s_e^2) - 4n^2 \pi^2 R_\pi^2 \right]^{1/2} \quad (6.61)$$

By using the CMB by COBE data in Chapter 4 and. Eq. (5.7), the approximate value of the proton core length was determined as:  $L_{pc} \approx 1.6277 \times 10^{-10}$  m. Giving proper numbers of turns  $n$ , we get a number of values  $L_{pc}$  around the approximately determined above value. These values are shown in Fig. 6.24 as a bar plot

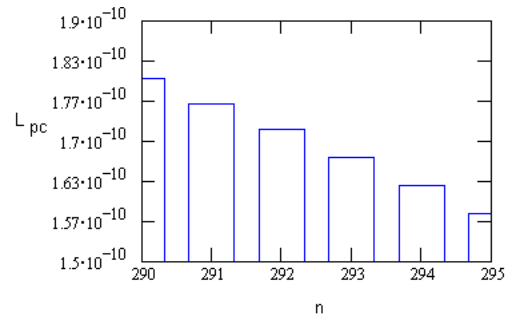


Fig. 6.24

Proton core length in function of pion turns

The most close value to 1.61E-10 m is this for turns of 294

$$L_{pc}(294) = 1.62772 \times 10^{-10} \text{ (m)} \quad (6.62)$$

The recalculated ZPE temperature corresponding to this value of  $L_{pc}$  is  $T = 2.7846 \text{ K}$ . This is 0.058 deg above the temperature determined by COBE (2.726 K). Having in mind, that the calculations are valid for the Earth local gravitational field, the small difference is reasonably contributed to the slightly larger ZPE of that field.

By the Eq. (6.61) we determined the accurate value of the proton length. **This is the length of the proton along its long axes, without taking into account the thickness of the external shell:**

$$L_p = 0.667 \times 10^{-10} \text{ (m)} - \text{proton length} \quad (7.62.a)$$

### 6.12.2.2 Some useful dimensions

Accepting  $n = 294$ , we get the following additional dimensions for the internal pion:

$$s_\pi = 5.5365 \times 10^{-13} \text{ (m)} \text{ second order step of the pion} \quad (6.63)$$

$$\frac{\sqrt{\left(2\pi \frac{2}{3} R_c\right)^2 + s_\pi^2}}{s_\pi} = 3.088 \quad \text{ratio of one turn length to second order step size of the internal pion} \quad (6.64)$$

$$\frac{2r_p}{L_{pc}} = 0.72435 \times 10^{-4} \quad \text{ratio of proton envelope thickness to core length} \quad (6.64.a)$$

### 6.12.2.3 Volume ratio between the proton envelope and the total volume of its FOHS's.

**The proton envelope is the smooth surface defined by its external positive shell.** The volume of the proton envelope participate in the ZPE balance in which the CL dynamic pressure and the CL space-time constant are both involved (see Chapter 5.).

Let  $R_{Vp} = V_{env}/V_{FOHS}$  is the volume ratio between the proton envelope and the total volume of its FOHSs. We may apply the mass equation for the proton and use  $R_{Vp}$  as a volume ratio. In order to eliminate the proton mass dependence of the electrical charge, we will use the mass of neutron instead of proton.

$$m_n = \frac{h v_c \pi (R_c + r_p)^2 L_{pc}}{c^2 2\pi^2 R_c r_e^2} \quad (6.65)$$

From Eq. (6.65) the factor  $R_{Vp}$  is directly determined.

$$R_{Vp} = \frac{h v_c (R_c + r_p)^2 L_{pc}}{c^2 2\pi R_c r_e^2} \frac{1}{m_n} = 71.72 \quad (6.66)$$

If the volume enclosed by the proton envelope was not accessible to the CL nodes, the factor  $R_{Vp}$  should be equal to unity. The obtained value, however, indicates, that the internal volume of the proton is accessible to CL nodes. Consequently:

**The internal volume of the proton (neutron) is filled with CL space.**

### 6.12.2.4 Verification of the dimensions by the newtonian mass equation

The general form of the newtonian inertial mass equation for a single helical structure is (see Chapter 3) is

$$m = \frac{P_S}{c^2} V_{H(SI)} \quad [(3.48)]$$

where:  $P_S$  is the CL static pressure and  $V_{H(SI)}$  is the FOHS volume (in SI units).

It has been noted that the equation in this shape is valid for FOHS with external negative shell. For FOHS with external positive shell additional multiplication factor of 2.25 must be used.

For compound structure as a proton and neutron the mass equation is simply the sum of masses of all the FOHSs' they contain.

$$m_{tot} = \Sigma m = \frac{P_S}{c^2} \Sigma V_{H(SI)} \quad (6.66.a)$$

The expression (6.66.a) can be applied for number of compound particles, composed of FOHS's whose mass is experimentally estimated. Having in mind that the proton (neutron) substructures are: pions and kaon, it is not difficult to guess the possible combinations of them. So operating by the volumes of one and same type of substructures and taking into account their possible modifications, the volumes of their FOHSs could estimated. Then the mass of the compound particle can be calculated by Eq. (6.66.a) and compared to the experimental measured value.

The correct charge balance for any compound particle will allow determination of correct number of pions pairs.

### A. Total mass equation applied for the proton (neutron)

When applying the mass equation for the proton, the volume  $V_H$  should be the total sum of all FOHS's., or  $V_H = V_{tot}$ . Having the volume ratio  $R_{Vp}$ , determined by Eq.(6.66), we can obtain the total volume of all FOHS's,  $V_{tot}$

$$V_{tot} = \frac{V_{env}}{R_{Vp}} = \frac{\pi(R_c + r_p)^2 L_{pc}}{R_{Vp}} = 1.0959 \times 10^{-36} \text{ (m}^3\text{)} \quad (6.67)$$

According to the mass equation (3.48) the sum of the newtonian masses of the separate FOHS' is equivalent to the sum of their volumes, multiplied by the factor  $\rho_{sc}^2$ . If we normalise the mass budget equation to this factor, we get the equation of the volume budget. In the case for the helical structures with external positive shell the correction factor of 2.25 should be applied for their volumes. The FOHS's volumes of the proton substructures are:

$$V_{\pi^-} = \pi(k_{RST}r_e)^2 L_{pc} \quad \text{FOHS volume of } \pi^- \quad (6.68)$$

$$V_{\pi^+ (cor)} = 2.25\pi(k_{RST}r_p)^2 L_{pc} \quad \text{corrected FOHS volume of } \pi^+ \quad (6.69)$$

$$V_{K0} = \pi(k_{RST}r_2)^2 L_{pc} \quad \text{volume of the neutral kaon} \quad (6.70)$$

$$V_{pext} = 2.25(2\pi^2 R_c r_p^2) n_t \quad (+) \text{ corrected volume of the external shell} \quad (6.71)$$

$$V_{\pi^-} = V_{\pi^+ (cor)} \quad \text{- corrected volume equivalence}$$

where:  $n_t$  - is the number of turns in the positive external shell

$k_{RST} = 1.1493$  - radius restoration factor for twisted FOHS (see§6.4.4.2)

After the proton break-up the pions and kaons are cut in one place only and their FOHSs have undergo fast twisting in which process the internal RL(R) are modified into (RL(T) and their FOHS volume get a slight decrease. The factor  $k_{rst}$  allows to restore the radius of FOHS envelope before the twisting, and consequently to obtain its former volume. This factor has been estimated by the twisting obtained after pion-muon conversion and referenced to the small radius  $r_p$  of the positron. The internal pions have some twisting even inside the proton and consequently anyone of the possessers a charge, but they are locked in proximity and

commonly neutralized. The internal kaon, however, is not twisted (this is evident from the mass difference between  $w^\pm$  and Z bozon, that in fact are destruction energies of untwisted and twisted RL structures). Consequently the internal kaon possessing RL(R) could not have strong negative charge and may only balance the internal positive field of the external shell of the proton. This means that the pions has to balance itself, so they must be in pairs. Then we have to check options with one pair, two pairs and so on.

The FOHS volume of the external positive shell is expressed by the volume of a single turn, multiplied by the number of turns  $n_t$ . The volume of the single turn of the external positive shell is equal to the free positron volume.

The total volume of all FOHSs involved in the proton expressed as a sum of corrected (from twisting) volumes of its substructures is:

$$V_{tot} = (V_{\pi^-} + V_{\pi^+}) n_{pair} + V_{K0} + V_{pext} \quad (6.72)$$

where:  $V_{\pi^-}$ ,  $V_{K0}$  and  $V_{pext}$  are respectively FOHS volume of pion, kaon, and external proton shell

$n_{pair}$  is the possible number of pion pairs

The value of  $V_{tot}$  by Eq. matches the value obtained by Eq. (6.72) for  $n_{pair} = 1$  (one pair of charged pions) and one straight negative FOHS with external RL(R-) and internal RL(R+). The same value of pair pions is in agreement with the results for eta particle and antiproton/proton stopping power, presented in Table 6.8.

### B. Mass correction factor for the neutral kaon

The experimentally determined mass of  $K_L^0$  (and all other kaons modifications) is overestimated because the existing jet of cut kaon is not taken into account (see §6.10.4 and Fig. 6.21). Substituting  $v_{H(SI)}$  by  $V_{K0}$  given by Eq. (6.70) we obtain a value of  $K_L^0$  mass, that converted in MeV is: 45.286 MeV. This is about 11 times smaller than the experimentally provided value by NIST: 497.672 MeV. So the necessary correction factor is:

$$k_{cor} = 10.99$$

The same correction factor could be obtained simply by the the equality of the ratio between newtonian masses and volumes of FOHS's:

$$\frac{m_{K0EX}/k_{cor}}{m_{\pi\pm}} = \frac{V_{K0}}{V_{\pi}}$$

where:  $m_{\pi\pm} = 139.5699$  MeV according to NIST data

**C. Mass equation applied for the eta particle**

The structure of the eta particle was discussed in § .. It contains one neutral kaon, and pair pions with opposite charges. All these structures are cut in one place. In this case the kaon possesses active jet and its real mass should be the experimental estimated mass of  $K_L^0$  divided by correction factor  $k_{cor}$ . Consequently, when estimating the total volume of all FOHSs in the proton (neutron) the participated kaon  $K_L^0$  volume should be divided by this factor:

$$V_{\eta} = V_{\pi^-} + V_{\pi^+}(cor) + V_{K0}/k_{cor} \tag{6.73}$$

where:  $k_{cor}$  - correction factor of the experimental estimated kaon mass due to the jet (see §6.10.4 and Fig. 6.21)

The Eq. (6.73) is given for one pion pair, but it could be checked for different number of pairs.

**D. Mass equation applied for the “antiproton”**

The structure of the “antiproton” was discussed in §. It contains one neutral kaon, and one negative pion. They are still closed helical structures (not cut). The whole structure may be more twisted than the normal proton. The corrected volume budget is:

$$V_{\bar{p}} = V_{\pi^-} + V_{K0} \tag{6.74}$$

**E. Mass equation applied for short lived “antiproton” containing cut kaon with jet**

Such antiproton could be involved in the experiment of measuring the stopping power ratio between “antiproton and proton. In such case the the kaon volume contribution should be corrected by the factor  $k_{cor}$ .

$$V_{\bar{p}} = V_{\pi^-} + V_{K0}/k_{cor} \tag{6.74.a}$$

**6.12.2.5 Calculated results**

According to the mass equation (3.48) the ratio of the corrected volumes from different FOHS’s is equal to the ratio of their newtonian masses. Then for the eta particle and the antiproton we have the relations

$$\frac{m_{\eta}}{m_p} = \frac{V_{\eta}}{V_{env}} \text{ for eta} \quad \frac{m_{\bar{p}}}{m_p} = \frac{V_{\bar{p}}}{V_p} \text{ for antiproton/ proton}$$

stopping power

The eta particle mass is accurately measured. The antiproton/proton stopping power is extensively investigated by M. Agnello et all. (1995) (a large group of co-investigators) for kinetic energy range from 0.5 KeV to 1.1 MeV. It is found that the ratio is about 65 %.

The obtained results are shown in Table .6.8.

**Table 6.8**

Para- meters	$n_{pair}$	$n_t$	$m_{\eta}$ (calc) [MeV/c <sup>2</sup> ]	$m_{\eta}$ (exp) [MeV/c <sup>2</sup> ]	SP ratio (calc.)	SP ratio (exp.)
	1	1204	602.6	583.31	0.678	(0.62 - 0.65)

*SP ratio - stopping power ratio between anti-proton and proton.*

The fractional error of the calculated mass of the eta particle is 3.5 %. The model provides additional parameters as : number of turns of the internal pion, step to radius ratio, pion to kaon FOHS length ratio. The value of the last parameter is 3.082. The most important parameter is the the proton core length, from where the proton length is determined. This parameter is verified and cross validated in Chapter 9.

Some useful parameters obtained by the model are the following:

**Internal pion**  
Number of turns: 294

Ratio between FOHS length of a single turn and the size of the second order step: 3.088

**External proton shell**  
Step to radius ratio of the SOHS: 0.3501

**Pion to kaon FOHS length ratio:** 3.0822

**Volume ratio of internal RL(T)**  
Between external positive shell and a positive kaon: ~ 30

Between pion and kaon same type of structures ~ 3.

Conclusion:

**The mass equation applied for the proton (neutron) indicates that it is comprised of one**

**not twisted central kaon (with external negative shell), two pions with opposite charges and external positive shell with internal structure of RL(T) type. The latter provides the positive charge of the proton.**

### 6.12.2.7 External dimensions of the proton structure

Relying on the accepted shape of Hippoped curve with parameter  $a = \sqrt{3}$ , one may determine the basic parameters of the proton dimensions: proton length; proton width and core thickness.

The core length was  $L_{pc}$  determined (see Eq. (6.62). The length of the Hippoped curve, corresponding, to  $L_{pc}$  is given by the integral:

$$L_{pc} = 2L_p \int_0^{\theta_{max}} \sqrt{(1 - a^2(\sin\theta)^2) + \frac{a^4(\sin\theta)^2(\cos\theta)^2}{1 - a^2(\sin\theta)^2}} d\theta \quad (6.75)$$

where:  $\theta_{max} = 0.19590657\pi$  - is a limit angle of integration

$L_p$  is the proton length;

The upper boundary of the integration  $\theta_{max}$  corresponds to the disectrice angle in [rad] at the origin of the curve.

The proton length  $L_p$  is determined from Eq. (6.75). The proton width is determined by the width of the Hippoped curve for  $a = \sqrt{3}$ . The proton core thickness is:  $2(R_c + r_p)$ .

*The calculated proton dimensions are:*

$$L_p = 0.667 \times 10^{-10} \text{ m} \text{ - proton length} \quad (6.76)$$

$$W_p = 0.19253 \times 10^{-10} \text{ m} \text{ - proton width} \quad (6.77)$$

$$2(R_c + r_p) = 7.9411 \times 10^{-13} \text{ m} \text{ - core thickness} \quad (6.78)$$

*Note:* The proton length and width are referenced to the central axis of the proton core.

### 6.12.3 Experimental confirmation about the theoretically determined proton dimensions

So far one experimental confirmation about the length of the proton core was used: the proton core length, cross calculated by the ZPE and CMB temperature. Additional verification of the proton external shape and dimensions are also possible, by using of:

(a) The Atomic Nuclear Atlas;

(b) The electron orbits around the protons in the atomic nuclei. (See the the orbital quasiplanes and Balmer series model in Chapter 7);

(c) The atomic nuclear configurations in the chemical compositions (Chapter 9);

(d) the internuclear distances, determined by X - ray crystallography (Chapter 8)

From all this cases, using the BSM interpretation, the proton length could be approximately verified.

In chapter 9, for example, the proton length appears apparent, from the 3D structure of the Chlorine molecule with a covalent bonds. The only needed parameter is the internuclear distance. The latter is known by the X - ray crystallography.

One example for the proton length verification, by using the Nuclear Atlas is the following:

Let to use the experimentally determined radius of the Neon atom estimated experimentally, but assuming a spherical shape. Looking at the configuration of the Ne atom in the Atomic Atlas we see that the pole to pole distance is just equal to the proton length. The electrons orbits in ground state does not contribute to the atomic radius. The atomic shape of Ne, in fact, is not sphere but oblate spheroid. In order to be able to use the estimated radius for Ne atom as a sphere, we will equate the volumes of sphere and obliterated spheroid.

$$\frac{4\pi a^2 b}{3} = \frac{4\pi R_s^3}{3} \quad (6.79)$$

where:  $a$  and  $b$  are the large and small obliterated spheroid radii, and  $R_s$  is a radius of the sphere

From the nuclei model of Ne, we see, that it could be inscribed in oblate spheroid with radius ratio:  $a/b = 1.805$ . Substituting  $a$  in Eq. (6.79) and solving for  $b$  we get

$$b = 0.67455 R_s. \quad (6.80)$$

Let to use the radius of Ne given by Michigan Institute of technology: <http://wulff.mit.edu/pt>

$$R_s = 0.51 \times 10^{-10} \text{ (m)}$$

$$\text{From Eq. (6.80) we get: } b = 0.344 \times 10^{-10} \text{ (m)}$$

Then the proton length is directly obtained as twice the smaller radius  $b$  of the spheroid envelope

$$L_p = 2b = 0.688 \times 10^{-10} \text{ (m)} \quad (6.81)$$

The proton length calculated by the Ne radius appears larger than the theoretical value (Eq. 6.76) by 3%, but this difference could be explained by the applied method of measurement in which the

electron orbits in the equatorial region of the Ne atom may contribute to the estimated dimensions. (The spatial position of the electron orbits of the inertial gazes become apparent in Chapter 8).

**The most strict verification of the proton length is obtained in Chapter 9 where the parameters  $L_p$  and  $W_p$  are involved in number of equations whose result show excellent agreement with some spectroscopic data of Hydrogen molecules.**

### 6.13 Neutron

Fig. 6.25 shows the external shape of the neutron. its external shell and internal structures are the same as the proton.

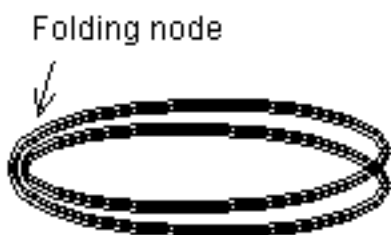


Fig. 6.25  
Neutron shape

The external shape of the neutron is characterized by a folding node of the core. The external helical shell of the core structure in the folding node does not penetrate each other. (This is not evident from the drawing shown in Fig. 6.25)

The structural difference between the proton and neutron is only the larger degree of twisting of all helical structures of the neutron. This means, that the neutron possesses a electrical field, however, it is locked by the IG field. The main reason for the locking of the electrical field is the shape of the neutron core. Due to the small thickness to core length ratio, the core shape is almost equivalent to two torus structures. Applying the graphical rule for cahрге of particle defined in §2.10.1.A. we will see that it could appear as a neutral particle.

#### 6.13.1 Neutron. Envelope shape and confined motion

Some of the features of the neutron has been already discussed in 6.1.4 The conversions be-

tween neutron and proton with emission of quasi-particle was also discussed in §6.2.

The free neutron is unstable and converts to a proton, because its intrinsic gravitation is not able to overcome the core elasticity in folded position. (Although when it is combined with proton, it stays in the proton saddle, and the intrinsic gravitation of the system is able to keep it in this position. This combination is a Deuteron). The free neutron has some equivalent helicity and exhibit confined motion. The interaction with the CL space in such motion helps it to preserve the overall shape and to prolong its lifetime. For this reason, the more energetic neutron has a longer life time. One additional factor keeping the neutron from conversion into a proton is the lattice resistance for creation or disappearance of the electrical charge (far electrical field).

There is one very particular feature of the neutron confine motion. When a monochromatic beam of neutrons passes through a crystal with parallel walls under Brewster angle, the outcome signal is separated in two beams in the same plane, but symmetrically deviated. The effect is known as Borman effect. The conditions of confined moving neutron when entering the crystal surface are illustrated by Fig. 6.26.

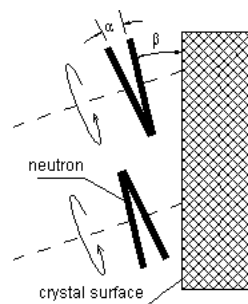


Fig. 6.26

The full explanation of the Borman effect is out of the scope of BSM, but some considerations will be pointed out.

- the angle of opening  $\alpha$  depends of the neutron velocity
- the Brewster angle  $\beta$  also depends of the neutron velocity
- there is two special cases in the moment when the neutron meet the surface of the crystal, and the phase difference between them is  $\pi$  For

both cases the folding node of neutron core yes in the drawing plane

d. when the folding node of the neutron core does not lie in the drawing plane, conditions for pendellosing effect occur.

### 6.13.2 Neutron-proton conversion and virtual particles

In the neutron to proton conversion process a positive charge appears as a far field and a negative wave is propagated as a virtual particle. In the proton to neutron conversion, the positive charge disappears and a negative quasiparticle wave is propagated as a virtual particle. In both cases the propagated virtual charge particle could be considered as a reaction of the CL space to the unlocked (or locked) electrical field. The physical explanation of the process is the following:

In case of photon emission, the lattice pumping is a result of multiple periodical oscillations. The pumped energy is well distributed between positive and negative nodes. In the case of proton/neutron conversion **the pumping is from aperiodical motion**. If the time duration of this motion is shorter than UL relaxation time (see Eq. ...), the pumped energy can not be equally distributed between the opposite CL nodes. Then this energy propagates through the CL space in a different way. The obtained wave affects the opposite nodes in non symmetrical way, exhibiting a feature of a moving charge. The configuration of the quasiparticle wave is little bit different than the quantum wave. It was described in Chapter 2, § Such wave could be deviated by electrical and magnetic field. **The major distinct feature by which the quasiparticle wave could be identified is its velocity - equal to the light velocity. It may be considered as a virtual electron.**

The quasiparticle wave, however, does not possess external boundary conditions and the quantum features are not so strong, as those of the quantum wave. For this reason we may accept, that the charge dissipate gradually. In such conditions, the rule of the charge unity may not be valid.

The proton-neutron or neutron-proton conversion is accessible for investigation by experiments. Apart of the neutronian mass change and the creation of quasiparticle wave, the reaction of CL

space includes additional energy, identified so far as a neutrino particle. Let to analyse the conversion of the free neutron to proton known as a Beta decay (of free neutron). In this process the neutron loses 1.294 MeV of its neutronian mass. But the unit charge of electron is 511 KeV. So the balance is:

$$1.294 \text{ MeV} = 511 \text{ KeV}(e+) + 511 \text{ KeV}(e-) + 272 \text{ KeV}$$

According to the BSM interpretation, the 511 KeV(e+) is a mass equivalent energy of the born positive charge, possessing by the proton. It reflects the volume change of all FOHS's in result of the twisting. The 511 KeV(e-) is the mass equivalent energy of the virtual electron and **272 KeV is a newtonian mass deficiency of the proton as a charge particle**. . This energy so far, has been contributed to the neutrino. According to BSM, however, this mass deficiency is the necessary energy to fulfil the balance of the IG forces for the twisted helical structure in CL space, according to Eq. (2.8). In a few words, the mass deficiency is an adjusting IG potential for a proton as a charge particle in CL space.

- **The energy of 272 KeV, related with the neutron/proton conversion is an adjusting balance energy of the CL space.**

The physical explanation of the mass deficiency effect is the following.

The neutron does not have electrical far field. This means that the positive and negative nodes in the far field are not biased and their SMP vectors participate equally for the propagation of intrinsic gravitation through the prisms core, forming the gravitational mass of neutron. When the structure is folded to a proton, the negative nodes of external surrounding field are engaged in motion of SMP vector in preferable direction aligned with the electrical lines. But the gravitational field is contributed from the equal distributed SMP vectors on the node quasisphere. The SMP motion serving the electrical field is removed from the total motion. In result of this, the particle suffer some portion of its gravitational mass. The proton is very large structure in comparison to node spacing and small percentage of the nodes are affected. The neutron and proton both are symmetrical structures, but during the conversion process they pass through not symmetrical shape. The charge birth or death has a finite time duration and during this process the following conditions are relevant:

(a) The neutron possesses a local gravitational field with spatial orientation determined by the folded node position. So the every neutron has a definite orientation in respect to the laboratory frame

(b) The spatial orientation of the obtained proton is correlated to the spatial orientation of the neutron

(c) The emission of the quasiparticle wave is correlated to the neutron - proton orientation

(d) The spatial direction of the proton momentum, obtained in result of the conversion, is correlated with the initial neutron orientation and the direction of the emitted quasiparticle wave.

The feature (d) is a measurable parameters in the experiments. It is known as “electron neutrino angular correlation effect.” The neutrino for beta decay has been introduced with purpose for conservation of the energy and angular momentum. It has not been directly observed in a beta decay process (and especially of free neutron), but only calculated by the energy balance. The energy balance, according to BSM interpretation is preserved, when taking into account the reaction of CL space. Consequently:

- **According to BSM, the  $\beta$  decay does not involve neutrino or antineutrino particle.**

The process of neutron proton conversion in beta decay in atoms is similar, but the energy range of the virtual particles is larger. The atomic nuclear is a complex structure of neutrons and protons following particular order and it could affect the energy of the virtual particles.

**It is well known fact that the average energy value for positive beta particles is slightly higher than the negative beta particles. The TP explanation for this difference is the following:** In the emission of positive beta (virtual) particles, the structure is moving from unfolded (proton) to folded (neutron) shape. In the final moment the intrinsic gravitation start to attract the structure parts and accelerate the folding process. In the opposite case the unfolded structure does not stop exactly at the proton shape but overpasses it aperiodically. An aperiodical motion in the first case is not possible. During the aperiodical motion some portion of the energy could be transferred to the nuclear sys-

tem.. **This energy will be missing from the energy of the emitted negative beta (virtual) particle.**

The BSM explanation of the mass deficiency effect in the neutron/proton conversion may provide explanation of the discrepancy between measured Solar neutrino flow and the calculated one.

### 6.13.3 Neutron in Deuteron

The external shape of the core is a characteristic feature of the proton and neutron. While the free neutron is not stable in CL space, it is quite stable when combined with a proton in a shape shown in Fig. 6.27 This is the shape of Deuteron. .

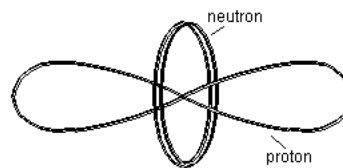


Fig. 6.27  
Deuteron nucleus

The combination effect of intrinsic gravitational forces of the proton and neutron make the structure very stable. The stabilizing effect of the proton structure on the neutron is obvious and do not need of explanation. Additional stabilizing factor, valid also for the free neutron is the CL space reaction on the appearance of far field electrical charge. The Deuteron is one of the basic component in the nuclear structures of the atoms.

### 6.13.4 Neutrons in Tritium

The tritium is formed of one proton and two neutrons over its saddle. The stabilizing effect for the neutron is similar as in the Deuteron, but the Tritium is not a stable element because:

- The two neutrons could not be very close because the repulsion of the locked electrical field in the close distance to the external shell
- The IG filed from the two neutrons affect the partially the proton shape invoking untwisting force. This may affect the distribution of the electrical field lines and finally could lead to losing of one neutron.

When the Tritium is connected to other structures in the atomic nuclei, however, the proton

shape is less affected and the Tritium structure appears quite stable.

### 6.13.5 Neutron magnetic moment

One specific feature of the neutron is the possession of magnetic moment despite of its charge neutrality. The magnetic moments of the basic atomic particles are given in Table 6.2.

Table 6.2

Particle or combinations	magnetic moment (JT <sup>-1</sup> )
neutron	$\mu_n = -0.96623707 \times 10^{-26}$
proton	$\mu_p = 1.41060761 \times 10^{-26}$
electron	$\mu_e = 9.28477 \times 10^{-24}$
deuteron	$0.43305 \times 10^{-26}$
tritium	$1.5045 \times 10^{-26}$

All the features, mentioned above, find their explanation by the BSM theory. The existence of the neutron magnetic moment has been already explained in Chapter ... **But why the neutron magnetic moment is opposite to those of the proton?**

In Chapter 5 §5.5.1 the electron magnetic moment was investigated and found that the change of prisms pitch angle of external shell affects the magnetic moment. The pitch angle should be referenced to the axis of particle confined motion. A similar effect could work for the neutron and proton. The neutron is closer to torus and its magnetic moment is defined by the average prisms pitch angle of its shell. When converted to a proton the pitch angle change. If the proton twisting was with the same handedness as its external shell, the magnetic moment will be larger but with a same sign. The fact that the magnetic moment change the sign means that the proton gets opposite higher order handedness. But the handedness of the proton twisting will be determined by the condition: which type of helical structure stiffness will predominate (right or left handed). Let to remember that the lower order helical structure has larger stiffness. But all the pions and kaon have negative central cores. The external shell of the proton (neutron) also possesses a negative core. Additionally the negative pion and the central kaon have a negative external shells. Then the negative structure stiffness will predominate. Following the rule that a core of left handed prisms will favour a left handed

twisting, we may conclude, that the twisted proton will get an opposite handedness of its external shell. This explains the sign change of the magnetic moment. In fact the handedness of proton twisting is predetermined by the proton-neutron. According to the above accepted consideration we obtain:

- the higher order handedness of the proton corresponds to the handedness of the negative prism

- the second order handedness of the electron and positron corresponds to the handedness of the negative prism

In Chapter ... we will see, that the atomic nuclear structure possesses a handedness, corresponding to the proton handedness. The structure analysis of the simple molecules also shows, that the handedness of the atoms is propagated to the molecules. Then we may consider, that the handedness of a complex molecule like the DNA corresponds to the handedness of the atoms, and consequently to the proton. It is proved that the DNA possesses a right-hand helicity. Then the proton should have the same handedness. From this follows, that the negative prism is right handed.

- **From the analysis of the above considerations it follows, that the negative prism is a right-handed.**

The author of BSM is not 100% sure about the above conclusion. So it must be additionally verified. For this reason in many cases a positive or negative attribute is used instead of more accurate one as left handed or right handed.

### 6.14 Neutrino particle classification

The neutrino firstly was introduced in connection with the Beta decay. Later additional types were accepted for muon to electron decay. Later, they have been experimentally detected from the space, from the Sun and from the nuclear colliders. Presently, the neutrino concept is not solved in satisfactory level, by the modern physics. Number of different type of neutrino are in discussion. The solar neutrino problem is not solved.

According to BSM, the accepted neutrino in the Beta decay does not have anything common with a real neutrino particle. In order to match the terminology we may call it "virtual neutrino", having in mind the above comment. In some processes,

both types are obtained simultaneously. The Table 6.3 gives the types of the neutrinos and their relation to some decay processes.

*Types of neutrinos according to BSM* **Table 6.3**

Type	From process
neutrino from partly folded RL node	FOHS destruction
neutrino from folded RL node	FOHS destruction (also from $\mu \rightarrow e$ )
“virtual” neutrino	$n \rightarrow p$ ; $\pi \rightarrow \mu$

The signature of the partly folded RL nodes in the

experiments might be the electroweak current, introduced by the electroweak theory. The neutrinos, detected by the neutrino detectors are from the folded RL nodes.

In  $n \rightarrow p$  process (neutron - proton conversion) only a twisting is involved. The energy that is detected by the obtained proton momentum is not a quantum wave and is dissipated in CL space, contributing to the ZPE. It comes from the Neutronian mass change, due to the shrinkage of the FOHS's. This energy currently is accepted (by the modern physics) as antineutrino particle.

In the  $\pi \rightarrow \mu \rightarrow e$  decay, there is a process of twisting, followed by FOHS destruction. So the “virtual” and real neutrinos appear almost simultaneously. This is the confusing feature, in result of which the “virtual “ neutrino is misidentified as a real neutrino. The neutrino detectors may detect only real neutrinos. In the present time their threshold level of detection is higher, than the energy of the antineutrino from the inverse Beta decay.

The first experiment, considered as a neutrino confirmation is provided by F. Reines, C. Cowan et al. They measure the “energy-mass” difference in the reaction  $p \rightarrow n$  and considered the missing part to be the signature of the neutrino. **Direct neutrino particle in this case is not measured.** (see Cl. Cowan, Jr, F. Reines et al. (1956). This signature is considered so far as a low energy neutrino. Later real neutrino particles has been detected, but directly by neutrino detectors. They , posses, however much higher energies From the BSM theory, we already know that the low energy “neutrino” is a signature of the Neutronian mass difference due to the untwisting, that changes the volume of all FOHS's. For this reason the BSM denoted is as a virtual neu-

trino, keeping in mind, that it does not have anything common with the real neutrino.

The processes of high Z number element building in the Sun are characterized with large number of  $n \rightarrow p$  type of reaction (the build-up process is described in Chapter 8). The energy of the “virtual” neutrino from this reaction is dissipated in the Sun local gravitational field. So the “virtual” neutrino is missing in the neutrino detectors used in the Earth. These detectors may catch only real neutrinos from the space or from the particle colliders. This might be explanation of the “solar neutrino deficit”.

In the high energy range, the neutrino detectors detects real neutrinos. **The neutrino emitted by supernova SN1987A has been discovered** by IBM (Irvine-Michigan-Brookhaven) Collaboration. The observation was led by Fred Reines. **This indicates, that in the supernova, processes of massive destruction of FOHS's take place.** In a cosmic scale such process may involve an unimaginable enormous energy.